Journal of Mathematical Sciences: Advances and Applications
Volume 6, Number 2, 2010, Pages 257-285

MATHEMATICAL INVERSE PROBLEM OF ELECTRIC AND VERTICAL MAGNETIC FIELDS TO RESOLVE THE SALINE SOIL STRUCTURE

PAGAMAS PAWONG and SUABSAGUN YOOYUANYONG

Faculty of Science
Silpakorn University
Nakornpathom 73000
Thailand
e-mail: suabkul@su.ac.th

Abstract

Joint inversion of the electric and vertical magnetic field responses due to a vertical magnetic dipole is performed by using the linearized theory of Backus and Gilbert in order to estimate the conductivity profile of saline soil, which is assumed to be a function of depth only. An initial apparent conductivity profile can be obtained to start the iteration off. The iterative procedure is found to be robust with respect to starting models. Within the confines of the linearity assumption, broad convergence criteria are adopted to give an optimal solution, which is necessarily non-unique. This optimal solution is perturbed so that the solution obtained is just acceptable under the criteria used. The perturbed solutions are used to obtain bounds within which the true solution may be expected to lie.

1. Introduction

The frequency sounding controlled-source electromagnetic method (CSEM) is a useful tool for exploring the subsurface of the earth. The

2010 Mathematics Subject Classification: 76U05, 76V05.

Keywords and phrases: inverse problem, joint, electric, magnetic.

This research is supported by the Centre of Excellence in Mathematics, the Commission on Higher Education, Thailand, and the Faculty of Science, Silpakorn University, Thailand.

Received October 23, 2010

electric and magnetic field responses obtained from a primary vertical magnetic dipole (VMD) constitute a data set, which can be inverted to provide some knowledge of the earth. Backus and Gilbert [1], [2] presented a linearized theory for solving geophysical inverse problems. The linearized theory of Backus and Gilbert has been used by Oldenburg [9] to generate continuous resistivity profiles by inverting potential differences measured from direct current resistivity sounding. Fullagar and Oldenburg [5] performed automatic inversion of horizontal loop electromagnetic (HLEM) frequency sounding measurements over a layered earth.

The objective of this paper is to present a technique whereby the electromagnetic observations obtained from a vertical magnetic dipole above the ground surface can be inverted to determine the conductivity model, which is a continuous function of depth. The linearized inverse theory of Backus and Gilbert [1], [2] is used to develop an iterative method for constructing the conductivity model, whose calculated responses are close to the observed values. A conductivity profile satisfying the data is constructed iteratively via successive perturbation of a starting model. Joint inversion of the electric and vertical magnetic field responses is used to estimate the conductivity profile. This resulting model is necessarily non-unique, and the edgehog method due to Jackson [6] is used to construct a band within which acceptable solutions may be found. Detail results from a theoretical example is presented.

2. Derivation of Electromagnetic Field

In this paper, we consider the reflection of radiation from a vertical magnetic dipole source of strength $me^{i\omega t}$ at height h above the ground surface. Cylindrical polar coordinates (r, θ, z) will be used with origin at the source point and z is taken to be positive downwards. The conductivity distribution below the ground is assumed to be continuous and depends only on depth. The electric field $E(r, z, \omega)$ is then purely azimuthal and depends on depth and horizontal distance from the dipole source, and ω is the angular frequency. The magnetic field radiate in the radial and vertical directions, and are denoted by H_r and H_z, respectively. The governing equations are [14]

$$i\omega\mu_0 H_r = \frac{\partial E}{\partial z}, \tag{2.1}$$

$$i\omega\mu_0 H_z = -\frac{1}{r}\frac{\partial(rE)}{\partial r}, \tag{2.2}$$

$$\frac{\partial H_r}{\partial z} - \frac{\partial H_z}{\partial r} = (i\omega\varepsilon_0 + \sigma)E + J_{s\,\theta}. \tag{2.3}$$

Here σ is the conductivity, μ_0 and ε_0 are the permeability and permittivity of free space, respectively, $J_{s\,\theta}$ is the source current density given by $I(\omega)a\delta(r-a)\delta(z)/r,$ and $I(\omega)$ is the current in a coil of small radius a. Eliminating H_r and H_z from the above equations, we obtain

$$\frac{\partial^2 E}{\partial z^2} + \frac{\partial^2 E}{\partial r^2} + \frac{1}{r}\frac{\partial E}{\partial r} - \frac{E}{r^2} - i\omega\mu_0(i\omega\varepsilon_0 + \sigma)E = i\omega\mu_0 J_{s\,\theta}. \tag{2.4}$$

Equation (2.4) may be simplified by introducing the Hankel transform of the electric field $\widetilde{E}(\lambda, z, \omega)$ as

$$\widetilde{E}(\lambda, z, \omega) = \int_0^\infty E(r, z, \omega) r J_1(\lambda r) dr. \tag{2.5}$$

The transformed field $\widetilde{E}(\lambda, z, \omega)$ satisfies the differential equation

$$\frac{\partial^2 \widetilde{E}}{\partial z^2} - (\gamma^2 + \beta)\widetilde{E} = i\omega\mu_0 a I(\omega) J_1(\lambda a)\delta(z), \tag{2.6}$$

where $\gamma^2 = \lambda^2 - \omega^2\mu_0\varepsilon_0,$ and $\beta = i\omega\mu_0\sigma(z).$ On neglecting displacement currents, we may replace γ by λ.

In air, the electric field, $\widetilde{E}_{air}$, is composed of a primary and secondary component, $\widetilde{E}^p$ and $\widetilde{E}^s$, respectively, where

$$\widetilde{E}_{air} = \widetilde{E}^{p} + \widetilde{E}^{s}.$$

The primary electric field can be solved by using Equation (2.6) for $\sigma = 0$, which gives [14]

$$\widetilde{E}^{p}(\lambda, z, \omega) = -\frac{i\omega\mu_0 a I(\omega) J_1(\lambda a) e^{-\lambda z}}{2\lambda}, \quad 0 < z < h. \tag{2.7}$$

Solving for the secondary electric field, the differential equation (2.6) becomes

$$\frac{\partial^2 \widetilde{E}^{s}}{\partial z^2} - \lambda^2 \widetilde{E}^{s} = 0. \tag{2.8}$$

The solution to Equation (2.8) is

$$\widetilde{E}^{s}(\lambda, z, \omega) = C_1 e^{\lambda z} + C_2 e^{-\lambda z}, \tag{2.9}$$

where C_1 and C_2 are arbitrary constants. The condition for $\widetilde{E}^{s}(\lambda, z, \omega)$ to be bounded, leads to $C_2 = 0$ and the electric field is given by

$$\widetilde{E}^{s}(\lambda, z, \omega) = C_1 e^{\lambda z}. \tag{2.10}$$

In the ground, Equation (2.6) becomes

$$\frac{\partial^2 \widetilde{E}}{\partial z^2} - (\lambda^2 + \beta)\widetilde{E} = 0, \quad z > h. \tag{2.11}$$

The integral solution to $\widetilde{E}(\lambda, z, \omega)$ can be determined by using the method of variation of parameters, which gives

$$\widetilde{E}(\lambda, z, \omega) = Be^{-\lambda z} - \frac{1}{2\lambda}\int_h^{\infty} \beta(\xi)\widetilde{E}(\lambda, \xi, \omega)K(z, \xi)d\xi, \tag{2.12}$$

where $K(z, \xi) = e^{-\lambda|\xi - z|}$, and B is an arbitrary constant, which can be determined from the continuity of $\widetilde{E}$ and $\frac{\partial \widetilde{E}}{\partial z}$ at the air-ground interface. For a dipole, it can be shown that $B = -(i\omega\mu_0 m)/(4\pi)$, where $m = \pi a^2 I(\omega)$ is the dipole moment.

The vertical magnetic field can be computed by applying Faraday's law to give

$$H(r, z, \omega) = \frac{i}{\omega\mu_0}\int_0^\infty \lambda^2 J_0(\lambda r)\widetilde{E}(\lambda, z, \omega)d\lambda. \tag{2.13}$$

3. Fr*é*chet Kernel Formulation

Following Backus and Gilbert [1], our procedure constructs a model iteratively by linearized improvement of a starting model. Fundamental to our construction scheme are the Fréchet kernels $F_e(r, z, \omega)$ and $F_{mz}(r, z, \omega)$, which relate changes in responses to a small change $\delta\sigma$ in the conductivity according to

$$\delta E = \int_0^\infty F_e(r, z, \omega)\delta\sigma(z)dz + 0\| \delta\sigma \|^2, \tag{3.1}$$

$$\delta H = \int_0^\infty F_{mz}(r, z, \omega)\delta\sigma(z)dz + 0\| \delta\sigma \|^2. \tag{3.2}$$

Following the method of Fullagar and Oldenburg [5], the Fréchet kernels for the tangential electric field and the vertical magnetic field are given, respectively, by

$$F_e(r, z, \omega) = \frac{2}{a^2 I(\omega)}\int_0^\infty \widetilde{E}^2(\lambda, z, \omega)\, e^{\lambda h} J_1(\lambda r)d\lambda, \tag{3.3}$$

$$F_{mz}(r, z, \omega) = \frac{i}{\omega\mu_0}\int_0^\infty F_e(\lambda, z, \omega)\lambda^2 J_0(\lambda r)d\lambda. \tag{3.4}$$

4. Apparent Conductivity Transformation

Since the tangential electric field, the vertical magnetic field and the Fréchet kernels contain the conductivity as a function of depth, we need the initial estimate of the corresponding conductivity profile from the measured data. Das [4] gave a scheme whereby the apparent conductivity as a function of distance r and frequency f (in hertz), where $\omega = 2\pi f$, can be obtained from the measured values of E and H_z. This is given by

$$\sigma_a(r, f) = \frac{\left|[\ln F(r, f)]^2\right|}{\omega\mu_0 r^2}, \tag{4.1}$$

where

$$F(r, f) = \frac{\sqrt{f}}{4}\int^{f} \frac{H_z^N(r, x) - 3E^N(r, x)}{x^{3/2}}\,dx.$$

Because the apparent conductivity derived by Das is not a function of depth, we need to find the relation between frequency and depth. The apparent conductivity as a function of depth will be normalized by the conductivity at the ground surface and used for the starting iterative model. The transformation of the apparent conductivity from a function of r and f to a function of r and z may be done using the sensitivity equation. Following Smith et al. [11], if $\widetilde{E}_h$ is the Hankel transform of the response due to a dipole source above a homogeneous earth, then the change on the surface $\delta\widetilde{E}$ due to a small change, $\delta\sigma(z)$ in the conductivity, is given by

$$\delta\widetilde{E} = -\frac{i\omega\mu_0}{2\lambda\widetilde{E}^p(\lambda, h, \omega)}\int_0^{\infty} \widetilde{E}_h^2(\lambda, z, \omega)\delta\sigma(z)dz. \tag{4.2}$$

Now, the solution to Equation (2.11) for a homogeneous half-space with constant conductivity is given by

$$\widetilde{E}_h(\lambda, z, \omega) = D_1 e^{u_1 z} + D_2 e^{-u_1 z}, \quad z > h,$$

where $u_1^2 = \lambda^2 + \beta$, and D_1 and D_2 are arbitrary constants. The condition for $\widetilde{E}_h(\lambda, z, \omega)$ to be bounded, leads to $D_1 = 0$ and the electric field is therefore given by

$$\widetilde{E}_h(\lambda, z, \omega) = D_2 e^{-u_1 z}. \tag{4.3}$$

The constant D_2 can be found from the boundary conditions at the air-ground interface as before giving

$$D_2 = -\frac{i\omega\mu_0 a I(\omega) J_1(\lambda a) e^{-\lambda h + u_1 h}}{\lambda + u_1}.$$

Hence, the solution for the electric field is

$$\widetilde{E}_h(\lambda, z, \omega) = -\frac{i\omega\mu_0 aI(\omega)J_1(\lambda a)e^{-\lambda h + u_1 h - u_1 z}}{\lambda + u_1}. \tag{4.4}$$

The sensitivity equation now reads

$$\delta\widetilde{E} = -\frac{\omega^2\mu_0^2 aI(\omega)J_1(\lambda a)e^{2u_1 h - \lambda h}}{(\lambda + u_1)^2}\int_0^\infty e^{-2u_1 z}\delta\sigma(z)dz. \tag{4.5}$$

If there is a change of $\sigma(z)$ at $z = z_1$ only and the change is $\delta\sigma(z) = \widetilde{d}(z_1)\delta(z - z_1)$, then the corresponding change in $\widetilde{E}_h$ due to this change in σ may be written as

$$\delta\widetilde{E}(\lambda, z_1, \omega) = -\frac{\omega^2\mu_0^2 aI(\omega)J_1(\lambda a)e^{2u_1 h - \lambda h - 2u_1 z_1}\widetilde{d}}{(\lambda + u_1)^2}, \tag{4.6}$$

where $\widetilde{d}$ is a scale factor proportional to the depth. Replacing z_1 by z in (4.6) and taking inverse Hankel transforms of (4.4) and (4.6) give

$$E(r, z, \omega) = -i\omega\mu_0 aI(\omega)\int_0^\infty \frac{J_1(\lambda a)J_1(\lambda r)\lambda e^{-\lambda h + u_1 h - u_1 z}}{\lambda + u_1}d\lambda, \tag{4.7}$$

$$\delta E(r, z, \omega) = -\omega^2\mu_0^2 aI(\omega)\widetilde{d}\int_0^\infty \frac{J_1(\lambda a)J_1(\lambda r)\lambda e^{-\lambda h + 2u_1 h - 2u_1 z}}{(\lambda + u_1)^2}d\lambda. \tag{4.8}$$

From now on, we will assume the dipole to be located on the surface of the earth $(h = 0)$. Normalizing $\delta E(r, z, \omega)$ by $E(r, 0, \omega)$, and allowing a to tend to zero, we have

$$\delta E^N(r, z, \omega) = -i\omega\mu_0\widetilde{d}\,\frac{\displaystyle\int_0^\infty \frac{J_1(\lambda r)\lambda^2 e^{-2u_1 z}}{(\lambda + u_1)^2}d\lambda}{\displaystyle\int_0^\infty \frac{J_1(\lambda r)\lambda^2}{(\lambda + u_1)}d\lambda}. \tag{4.9}$$

The normalized sensitivity is plotted against depth (Figure 4.1) for a scale factor proportional to the depth given by $\widetilde{d} = bz$, where b is a constant (Smith et al. [11]). In this case, 8 normalized curves from 8 frequencies will be used to find the relation between frequency and depth at the maximum sensitivity. On each curve, there is a distinct peak at the depth, where a perturbation in conductivity will have a significant influence on the field response. This is the depth we choose to associate with the apparent conductivity. For f less than about 10^6, the depth of this peak decreases with increasing frequency. In Figure 4.2, the depth is scaled by $f^{-(1/2)}$. Here, we see that the scaled depth of maximum sensitivity increases as we increase the frequency and approaches a fixed value for f greater than about 10^6. The scaled depth for maximum sensitivity is plotted as a function of the frequency in Figure 4.3, which can be used for determining the depth corresponding to a particular frequency.

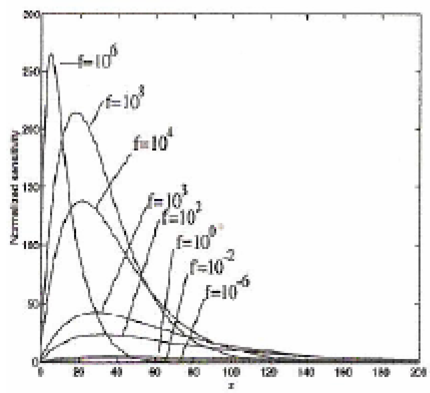

Figure 4.1. Curve of normalized sensitivity against depth.

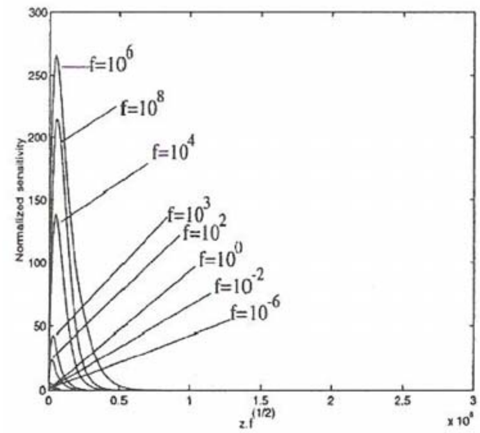

Figure 4.2. Curve of normalized sensitivity against $zf^{(1/2)}$.

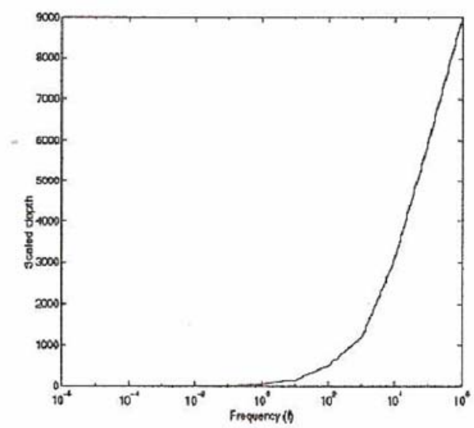

Figure 4.3. Curve of scaled depth of maximum sensitivity against frequency.

5. Non-Dimensional Variables and Iteration Process

The tangential electric field, the vertical magnetic field, the Fréchet kernels, and the apparent conductivity will be scaled and non-dimensionalized to avoid errors caused by the computation of small values. Introducing $\widetilde{U}(\lambda, z, \omega) = \widetilde{E}(\lambda, z, \omega) / B$, Equation (2.12) can be rewritten as

$$\widetilde{U}(\lambda, z, \omega) = e^{-\lambda z} - \frac{1}{2\lambda}\int_h^\infty \beta(\xi)\widetilde{U}(\lambda, \xi, \omega)K(z, \xi)d\xi. \tag{5.1}$$

Using L as the length scale, Ω as a reference angular frequency and scaling $E(r, z, \omega)$ and $H_z(r, z, \omega)$ by their corresponding free space values, namely, $E^0 = -i\omega\mu_0 m / 4\pi r^2$ and $H_z^0 = -m / 4\pi r^3$, respectively, the non-dimensional electric and vertical magnetic fields are given by

$$E^*(r^*, z^*, \omega^*) = (r^*)^2\int_0^\infty \lambda^* J_1(\lambda^* r^*)U(\lambda^*, z^*, \omega^*)d\lambda^*, \tag{5.2}$$

$$H_z^*(r^*, z^*, \omega^*) = -(r^*)^3\int_0^\infty \lambda^{*^2} J_0(\lambda^* r^*)U(\lambda^*, z^*, \omega^*)d\lambda^*, \tag{5.3}$$

where an asterisk denotes a non-dimensional quantity. The corresponding expressions for the Fréchet kernels given by Equations (3.3) and (3.4) become

$$F_e^*(r^*, z^*, \omega^*) = -(\omega^*)^2\int_0^\infty J_1(\lambda^* r^*)U^2(\lambda^*, z^*, \omega^*)d\lambda^*, \tag{5.4}$$

$$F_{mz}^*(r^*, z^*, \omega^*) = -i\omega^*\int_0^\infty \lambda^* J_0(\lambda^* r^*)U^2(\lambda^*, z^*, \omega^*)d\lambda^*. \tag{5.5}$$

The non-dimensional apparent conductivity $\sigma_a^*(z^*)$ can be obtained by scalling the apparent conductivity, $\sigma_a(z)$, with the apparent conductivity at the ground surface $\sigma_a(0)$. $\delta\sigma^*(z^*)$ may be written as a linear combination of the Fréchet kernels (see, Backus and Gilbert [1]) to give

$$\delta\sigma^*(z^*) = \begin{cases} \displaystyle\sum_{j=1}^N \alpha_j^e F_{e_j}^*(z^*), & \text{for electric field,} \\ \displaystyle\sum_{j=1}^N \alpha_j^H F_{mz_j}^*(z^*), & \text{for vertical magnetic field,} \end{cases} \tag{5.6}$$

where α_j^e and α_j^H are constants determined from

$$\delta\widetilde{E}_j^* = \sum_{k=1}^{N} \alpha_k^e \int_0^\infty F_{e_j}^*(z^*)F_{e_k}^*(z^*)dz^*, \tag{5.7}$$

$$\delta\widetilde{H}_j^* = \sum_{k=1}^{N} \alpha_k^H \int_0^\infty F_{mz_j}^*(z^*)F_{mz_k}^*(z^*)dz^*. \tag{5.8}$$

$\delta\widetilde{E}_j^*$ and $\delta\widetilde{H}_j^*$ are the differences of the non-dimensional observation and calculation fields, and subscripts j indicate the field value at frequency ω_j^*. Eliminating α_j^e and α_j^H in Equations (5.6), (5.7), and (5.8), we have, in matrix from,

$$(\mathbf{B_e A_e^{-1}})\delta\sigma^* = \delta\mathbf{E}^*, \tag{5.9}$$

$$(\mathbf{B_H A_H^{-1}})\delta\sigma^* = \delta\mathbf{H}^*, \tag{5.10}$$

where $\mathbf{B_e}$, $\mathbf{B_H}$, $\mathbf{A_e}$, and $\mathbf{A_H}$ are matrices and the jk-th entry are defined by $\int_0^\infty F_{e_j}^*(z^*)F_{e_k}^*(z^*)dz^*$, $\int_0^\infty F_{mz_j}^*(z^*)F_{mz_k}^*(z^*)dz^*$, $F_{e_k}^*(z_j{}^*)$, and $F_{mz_k}^*$ $(z_j{}^*)$, respectively. From now on, matrices and vectors are denoted by bold letters, while their entries are referred to by the corresponding subscripted variables. Combining (5.9) to (5.10), we get

$$\mathbf{B}\delta\sigma^* = \mathbf{C}, \tag{5.11}$$

where

$$\mathbf{B} = \begin{pmatrix} \mathbf{B_e A_e^{-1}} \\ \mathbf{B_H A_H^{-1}} \end{pmatrix}, \quad \mathbf{C} = \begin{pmatrix} \delta\mathbf{E}^* \\ \delta\mathbf{H}^* \end{pmatrix}.$$

The elements of matrices **B** and **C** are complex quantities, while the density profile is real. We will use the simple expedience of separating the real and imaginary parts of **B** and **C** and replacing Equation (5.11) by another matrix equation

$$\mathbf{A}\delta\sigma^* = \mathbf{y}, \tag{5.12}$$

where all quantities are real and the number of rows of the matrix **A** is twice that of **B**. For convenience, we will now assume **A** to be an $m \times n$ matrix $(m > n)$, and the **y** vector contains the real and imaginary parts of the deviations from the observed fields. The matrix **A** changes with each iteration since the entries are functions of $\sigma^{*(\mathbf{k})}$ and this adds to the length of time required for the process to converge. In practice, each observed datum is the realization of a random variable, whose real and imaginary parts have variances, which are not necessarily equal. The values at the surface is in fact the only observable quantities. Because of the inherent non-uniqueness of the inverse problem, there will always be a certain amount of misfit in the solution. This measure of misfit may be characterized by the measure

$$\chi^2 = \sum_{i=1}^{m} \frac{y_i^2}{s_i^2}, \tag{5.13}$$

where s_i^2 is the corresponding variance of the observed quantity. The linearity assumption implicit in the derivation of the Fréchet kernel assumes that terms of order $\|\delta\sigma^*\|^2$ are small. To ensure that this linearity assumption is satisfied, we will limit the variation in $\delta\sigma_i^*$ to within $\pm\tau_i$, once the process is close to convergence. This also serves to limit the variance on the conductivity corrections. At the $(k+1)$-th step, τ_i may be choosen to be $\frac{1}{2}\sigma_i^{*(k)}$ for each i. This leads to the following measure for the smoothness of the solution (see, Jackson [6]):

$$S^2 = \sum_{i=1}^{n} \frac{x_i^2}{n}, \tag{5.14}$$

where $x_i = \delta\sigma_i^* / \tau_i$ and S^2 is normally taken to be small. Using the standardized variables x_i, $i = 1, 2, \ldots, n$ and $Y_j = y_j / s_j$, $j = 1, 2, \ldots, m$, Equation (5.12) is replaced by

$$\hat{\mathbf{A}}\mathbf{x} = \mathbf{Y}, \tag{5.15}$$

where the ij-th entry of the matrix $\hat{\mathbf{A}}$ is obtained by multiplying the corresponding entry in $\mathbf{A}$ by τ_j / s_i. As stated above, a new matrix $\hat{\mathbf{A}}$ is computed at each iteration and the algorithm used is equivalent to solving iteratively for the vector $\mathbf{x}^{(\mathbf{k}+1)}$ given $\mathbf{Y}^{(\mathbf{k})}$. Typically, the trial solution satisfies $\mathbf{x}^{(\mathbf{k}+1)} = \mathbf{VS}^{+}\mathbf{U}^{\mathbf{T}}\mathbf{Y}^{(\mathbf{k})}$, where $\hat{\mathbf{A}} = \mathbf{USV}^{\mathbf{T}}$ is the singular value decomposition of $\hat{\mathrm{A}}$, $\mathbf{S}$ is the matrix containing the singular values of $\hat{\mathrm{A}}$ and $\mathbf{S}^{+}$ is the pseudo inverse of $\mathbf{S}$. $\mathbf{U}$ and $\mathbf{V}$ are, respectively, the orthogonal matrices containing the eigenvectors of $\hat{\mathbf{A}}\hat{\mathbf{A}}^{\mathbf{T}}$ and $\hat{\mathbf{A}}^{\mathbf{T}}\hat{\mathbf{A}}$ (Daniel and Nobel [3]). In the iteration process, we will adopt as the stopping criteria of the following:

$$\chi^2 < m + \sqrt{2m}, \tag{5.16}$$

$$S^2 < 1. \tag{5.17}$$

The first condition states that the converged solution should be within one standard deviation of the mean of the random variable, while the second is a measure of the smoothness we are prepared to accept. When both criteria (5.16) and (5.17) are satisfied, we would have an optimal vector $\mathbf{x}^*$ corresponding to the final vector $\mathbf{Y}^*$. At the end of the k-th iteration, the optimal values of $\delta\sigma_i^* = \delta\sigma^*(z_i^*) = x_i^*\tau_i$ are used to give an improved estimate of the conductivity profile,

$$\sigma_i^{*(k+1)} = \sigma_i^{*(k)} + \delta\sigma_i^*. \tag{5.18}$$

The small change $\delta\sigma_i^*$ can be large and of opposite sign at adjacent depth points. To keep the oscillations under control, we smooth $\delta\sigma_i^*$ with a three-point averaging filter (weights: 0.25, 0.50, 0.25) when it is greater than 0.5. The filter is usually applied one or more times. When large perturbations of $\sigma_i^{*(k+1)}$ occurs, the new model is also smoothed by applying the filter one or more times. This gives a new conductivity model as defined by (5.18). Using this, new Fréchet kernels are obtained and the whole process is repeated.

6. Appraisal

Because of the non-uniqueness of the inverse problem, there is an infinite number of conductivity functions close to $\sigma^*(\mathbf{z})$, which will fit the data. Backus and Gilbert [2] provided an excellence tool for characterizing non-uniqueness by use of an averaging kernel $A(z, z_0)$. However, there are some limitations on that method, for instance, it has no meaning when the averaging function does not give a sufficiently narrow peak and the process is computation intensive. An alternative approach was considered by Jackson [6], in his edgehog method, where by the solution obtained is perturbed until it barely satisfies the convergence criteria, thus giving a band within which acceptable solutions may be found. Returning to Equation (5.15), if the non-zero singular values of $\hat{\mathbf{A}}$ are $\mu_1, \mu_2, \dots, \mu_p$, $p \leq n$, the error vector is given by

$$\epsilon = \mathbf{Y}^* - \hat{\mathbf{A}}\mathbf{x}^* = (\mathbf{I} - \mathbf{P})\mathbf{Y}^*, \tag{6.1}$$

where $\mathbf{P} = u_1 u_1{}^T + u_2 u_2{}^T + \dots + u_p u_p{}^T$ is an idempotent symmetric matrix and u_i is the i-th column of the matrix $\mathbf{U}$. By convention, we assume the singular values have been arranged in decreasing order of magnitude, so that $\mu_1 \geq \mu_2 \geq \dots \geq \mu_p$. The root mean square error r satisfies

$$\frac{mr^2}{\mathbf{Y}^{*\mathbf{T}}\mathbf{Y}^*} = \frac{\epsilon^{\mathbf{T}}\epsilon}{\mathbf{Y}^{*\mathbf{T}}\mathbf{Y}^*} = \frac{\mathbf{Y}^{*\mathbf{T}}(\mathbf{I} - \mathbf{P})\mathbf{Y}^*}{\mathbf{Y}^{*\mathbf{T}}\mathbf{Y}^*}.$$

The right hand side of this equation is Rayleigh's quotient, and since $\mathbf{I} - \mathbf{P}$ is also idempotent, we have that

$$mr^2 \leq \mathbf{Y}^{*\mathbf{T}}\mathbf{Y}^*. \tag{6.2}$$

Using (5.16), we now have that

$$r \leq 1 + \frac{1}{\sqrt{2m}}. \tag{6.3}$$

Thus, reducing the bound for χ^2 would reduce the root mean square error in the solution. The bound on the residue in terms of the original field vector **y** bears a very simple relation to the above. In fact, if Σ is the diagonal matrix with entries $[s_1, s_2, \ldots, s_m]$, then

$$\Sigma\, \mathbf{Y} = \mathbf{y} \quad \text{and} \quad \Sigma\, \hat{\mathbf{A}}\mathbf{T}^{-1} = \mathbf{A}.$$

The residue $\epsilon^{(0)}$ for the field quantity is given by

$$\epsilon^{(0)} = \mathbf{y} - \mathbf{A}\delta\sigma = \Sigma\left(\mathbf{Y} - \hat{\mathbf{A}}\mathbf{x}\right),$$

giving

$$\epsilon^{(0)^{\mathbf{T}}}\epsilon^{(0)} = \epsilon^{\mathbf{T}}\, \Sigma^{\mathbf{T}}\, \Sigma_{\epsilon}\,. \tag{6.4}$$

If $r^{(0)}$ denotes the root mean square error in terms of the field vectors, then use of Rayleigh's quotient on (6.4) now yields

$$r^{(0)} \leq \left(\max_i s_i\right)\mathbf{r}. \tag{6.5}$$

Returning to (6.1), we see that the error vector becomes zero, if **P** equals the $m \times m$ identity. This is achieved when $p = m = n$, in which case the optimal solution is the unique solution to the system. When $p = n < m$, the column of $\hat{\mathbf{A}}$ are independent and the optimal solution is the least square solution given by $\left(\hat{\mathbf{A}}^{\mathbf{T}}\hat{\mathbf{A}}\right)^{-1}\hat{\mathbf{A}}^{\mathbf{T}}\mathbf{Y}$. For $p < n$, the solution is not unique. A well known theorem (see, Daniel and Nobel [3], p. 348) states that if $\|\epsilon\|_2$ is minimized by $\hat{\mathbf{x}}$, any other vector of the form

$$\overline{\mathbf{x}} = \hat{\mathbf{x}} + \mathbf{v}^{(0)}, \tag{6.6}$$

where $\mathbf{v}^{(0)}$ is an arbitrary linear combination of the last $n - p$ columns of **V** will give the same minimum. In our procedure, our optimal set of vectors $\mathbf{x}^*$ and $\mathbf{Y}^*$ are obtained based on criteria (5.16) and (5.17) rather than on the minimization of $\|\epsilon\|_2$. Since $\mathbf{x}^*$ is spanned by the first p columns of **V**, what we ended up with is a vector different from that given by (6.6). In what follows, we will assume the final matrix $\hat{\mathbf{A}}$ to be the linear map used to approximate the non-linear relation between $\mathbf{x}^*$ and $\mathbf{Y}^*$. Since the orthonormal columns of $\mathbf{U}$ span $\mathbb{R}^{\mathbf{m}}$, let

$$\mathbf{Y}^* = \mathbf{U}\beta^* \quad \text{or} \quad \mathbf{U}^{\mathbf{T}}\mathbf{Y}^* = \beta^* \tag{6.7}$$

represent the coordinatization of $\mathbf{Y}^*$ in the column space of $\mathbf{U}$. The optimal vector is given by

$$\mathbf{x}^* = \mathbf{V}\mathbf{S}^+\mathbf{U}^{\mathbf{T}}\mathbf{Y}^* = \mathbf{V}\mathbf{S}^+\beta^*. \tag{6.8}$$

If

$$\mathbf{x} = \mathbf{V}\alpha \quad \text{or} \quad \mathbf{V}^{\mathbf{T}}\mathbf{x} = \alpha \tag{6.9}$$

is the coordinatization of $\mathbf{x}$ in the column space of $\mathbf{V}$, we see from (6.8) that

$$\mathbf{x}^* = \mathbf{V}\hat{\alpha}, \tag{6.10}$$

where $\hat{\alpha}_i = \beta_i / \mu_i$, $i \leq p$ and $\hat{\alpha}_i = 0$ for $i > p$. Writing $\beta^* = \hat{\beta} + \beta^{(0)}$, where

$$\hat{\beta}_i = \begin{cases} \beta_i^*, & \text{for } i \leq p, \\ 0, & \text{for } i > p. \end{cases}$$

We see that $\beta^{(0)}$ does not contribute to the derivation of $\mathbf{x}^*$. It can be shown also that

$$\| \epsilon \|_2^2 = \left\| \beta^{(0)} \right\|^2 + \left\| \mathbf{S}\hat{\alpha} - \hat{\beta} \right\|^2,$$

so that $\beta^{(0)}$ does contribute to the magnitude of the residue error. We have assumed that the data values are statistically independent, so that in term of the standardized variables, the variance in $\mathbf{x}^*$ is given by

$$\operatorname{Var}(x_i^*) = \sum_{j=1}^{m} \left(\hat{\mathbf{A}}_{ij}^+\right)^2 = \sum_{j=1}^{p} \left(\frac{V_{ij}}{\mu_j}\right)^2,$$

where $\hat{\mathbf{A}}^{+} = \mathbf{VS}^{+}\mathbf{U}^{\mathbf{T}}$ is the pseudoinverse of $\hat{\mathbf{A}}$ and subscripts *ij* denote the appropriate entry of the matrix. This variance can be large if some of the μ_j's are small, which in turn makes the uncertainty in the solution vector large. As remarked by Wiggin [13], the characteristic values of **A** in most inverse problems decrease exponentially, but there is not easy means of deciding when μ_j is too small. This also means that there may be huge uncertainties in the optimal vector $\mathbf{x}^*$. One solution is to limit the variance in x_i^* by adopting a threshold value t_q, defined by

$$\sum_{j=1}^{q}\left(\frac{V_{ij}}{\mu_j}\right)^2 < t_q, \tag{6.11}$$

and treating μ_j as zero for $j > q$. This effectively changes $\mathbf{S}^+$ and $\mathbf{x}^*$. To understand the significance of this, consider the solution to (5.15) given by

$$\mathbf{x}^* = \hat{\mathbf{A}}^{+}\mathbf{Y} = \hat{\mathbf{A}}^{+}\hat{\mathbf{A}}\mathbf{x},$$

where $\hat{\mathbf{A}}^{+}\hat{\mathbf{A}} = \mathbf{VS}^{+}\mathbf{SV}^{\mathbf{T}} = v_1 v_1{}^T + v_2 v_2{}^T + \ldots + v_p v_p{}^T$, and v_i is the i-th eigenvector in **V**. When $p = n$, $\hat{\mathbf{A}}^{+}\hat{\mathbf{A}}$ is the $n \times n$ identity and the solution vector is well resolved. (6.8) shows that the optimal solution is spanned by the columns of **V**. When $p < n$, then only the first *p* columns of **V** are required to produce the solution, which is now less well resolved. By reducing the number of columns of **V** used to produce $\mathbf{x}^*$, we are in fact sacrificing resolution for less uncertainty in the solution vector. On the other hand, we have

$$\hat{\mathbf{A}}\mathbf{x}^* = \hat{\mathbf{A}}\hat{\mathbf{A}}^{+}\mathbf{Y} = \mathbf{USS}^{+}\mathbf{U}^{\mathbf{T}}\mathbf{Y} = \mathbf{PY},$$

which is equal to **Y**, if $p = m(= n)$ giving perfect fit to the data. When $p < m$, the fitted data uses only the first *p* columns of **U**. Reducing the number of columns of **U**, that is used to form the matrix **P**, will affect the residue. Now, by construction, $x_i = \delta\sigma_i^* / \tau_i$ means that x_i cannot vary by more than 1 unit, so that it would be meaningless, if the variance is much greater than 0.1 say. This is then taken to be t_q and q is found, so that (6.11) is satisfied for all x_i^*. Given that the solution is not unique, a relevant question is whether we can vary $\mathbf{x}^*$ without violating criteria (5.16) and (5.17). Since $\mathbf{x}^*$ is in the subspace spanned by the first q columns of $\mathbf{V}$, perturbing $\mathbf{x}^*$ is equivalent to changing the linear combination of these q columns. This is the method used by Jackson [6] to obtain marginal models in his "edgehog method". The difference in the present approach is that the link between $\hat{\alpha}$ and $\hat{\beta}$ is maintained. Let

$$\mathbf{Y}^{*\mathbf{T}}\mathbf{Y}^* = M_0 < m + \sqrt{2m} = M, \quad \mathbf{x}^{*\mathbf{T}}\mathbf{x}^* = n_0 < n.$$

Suppose $\mathbf{x}^*$ is now perturbed by perturbing $\hat{\alpha}$ in (6.10). Let

$$\overline{\alpha} = \mathbf{D}\hat{\alpha},$$

where $\mathbf{D} = \operatorname{diag}(d_1, d_2, \ldots, d_q, 1, 1, \ldots, 1)$ is an $n \times n$ diagonal matrix, then the perturbed solution is

$$\overline{\mathbf{x}} = \mathbf{V}\mathbf{D}\hat{\alpha} = \mathbf{V}\overline{\alpha}.$$

$\hat{\beta}_i$ is now replaced by

$$\overline{\beta}_i = \mu_i \overline{\alpha}_i = \mu_i d_i \hat{\alpha}_i, \quad i \leq q,$$

while $\beta^{(0)}$ remains unchanged, and $\overline{\mathbf{Y}} = \overline{\beta} + \beta^{(0)}$. We consider as our marginal model, when either

$$\overline{\mathbf{Y}}^{\mathbf{T}}\overline{\mathbf{Y}} = M, \quad \overline{\mathbf{x}}^{\mathbf{T}}\overline{\mathbf{x}} < n,$$

hold, or

$$\overline{\mathbf{Y}}^{\mathbf{T}}\overline{\mathbf{Y}} < M, \quad \overline{\mathbf{x}}^{\mathbf{T}}\overline{\mathbf{x}} = n.$$

This means

$$\overline{\alpha}^{\mathbf{T}}\mathbf{S}^{\mathbf{T}}\mathbf{S}\overline{\alpha} \leq M - \beta^{(0)^{\mathbf{T}}}\beta^{(0)}, \quad \overline{\alpha}^{\mathbf{T}}\overline{\alpha} \leq n, \tag{6.12}$$

with equality holding in one case only. Both relations represent regions inside some ellipsoid centred at the origin, and hence there are always vectors lying on one surface and inside the other. The principal axes of the ellipsoids are the q leading orthonormal eigenvectors in $\mathbf{V}$. Following Jackson, we will consider perturbing one component of $\hat{\alpha}$ at a time. This would give the maximum amount that particular component can be perturbed, while keeping the other components fixed. The resulting bounds on $\overline{\mathbf{x}}$ will contain information regarding the range of x-values that can be reliable resolved. The amount of any component of $\hat{\alpha}$ may be perturbed can be obtained easily. Consider the case, where $d_j = 1$ for all $j \neq k$, and $d_k^2 > 1$. From (6.12), we have

$$\mu_k^2 \hat{\alpha}_k^2 (d_k^2 - 1) \leq M - M_0, \quad \text{and} \quad \hat{\alpha}_k^2 (d_k^2 - 1) \leq n - n_0, \tag{6.13}$$

which means either

$$\frac{M - M_0}{\mu_k^2} < n - n_0 \quad \text{or} \quad \frac{M - M_0}{\mu_k^2} > n - n_0, \tag{6.14}$$

depending whether the first or the second relation in (6.13) is an equality. If the first relation holds, then

$$d_k^2 - 1 = \frac{M - M_0}{\mu_k^2 \hat{\alpha}_k^2}, \tag{6.15}$$

otherwise,

$$d_k^2 - 1 = \frac{n - n_0}{\hat{\alpha}_k^2}. \tag{6.16}$$

7. Example Inversion

In our example, we simulate reflection of radiation data at distance 100 meters from a vertical magnetic dipole source, which is located on the ground surface. The conductivity distribution of saline soil below the ground is assumed to be continuous and depends only on depth. In this paper, the continuous conductivity model is used and given by

$$\sigma(z) = 0.02 + \frac{900}{150\sqrt{2\pi}}\, e^{-\left(\frac{z-200}{600}\right)^2}.$$

The tangential electric field and vertical magnetic field are generated by the forward problem and, to simulate real data, the theoretical values are perturbed by superimposing a Gaussian relative error to the three percent level. The associated errors can be regarded as realizations of normal random variables with zero means and variances s_i^2, $i = 1, 2, \ldots, m$. The apparent conductivity as a function of frequency is obtained using 101 different frequencies and is shown in Figure 7.1, where a spline has been passed over the data points.The transformed data, which give the conductivity as a function of depth is shown in Figure 7.2, together with the true conductivity profile. We note that the starting model shows a much shallower peak. The inversion process described earlier is now used, and 8 iterations are required to obtain the optimal solution.

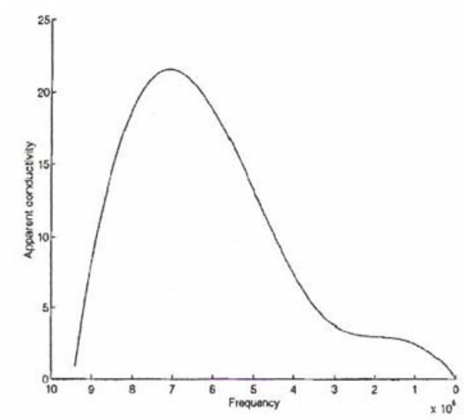

Figure 7.1. Curve of apparent conductivity against frequency.

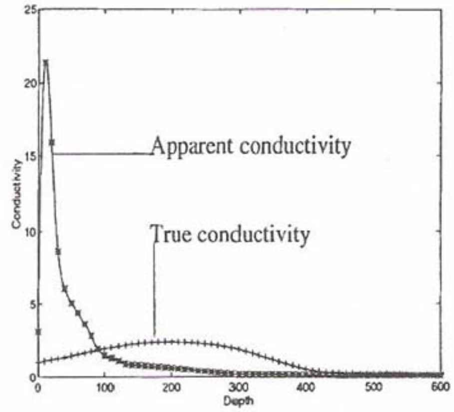

Figure 7.2. Curves of true and apparent conductivity against depth.

Figure 7.3 shows the conductivity profile obtained at the end of each iteration. The measure of misfit, χ^2 and the value of S are also given in Figure 7.3(h). Figure 7.4 shows the accepted model when only the tangential electric field data is used. In this case, 13 iterations are required. Similarly, Figure 7.5 shows that 11 iterations are required, if only the vertical magnetic field data are used. These illustrate the advantage in using joint inversion as commented by some other authors (for example, Jupp and Vozoff [7], Vozoff and Jupp [12], Raiche et al. [10], and Meju [8]). Figure 7.2 shows that the starting model is very different from the true conductivity profile. If the iterative process is robust, it should converge for a wide range of starting models. To show the robustness of the iterative process, a constant conductivity profile, $\sigma(z) = \sigma_a(0)$ is also used as a starting model and after 8 iterations, we again arrive at an acceptable model as shown in Figure 7.6. The conductivity profiles are shown up to a depth of 600 meters only because at this depth, the magnitude of the Fréchet kernel has decayed to a very small fraction, 10^{-9}, of their peak value. Figure 7.3(h) and Figure 7.6

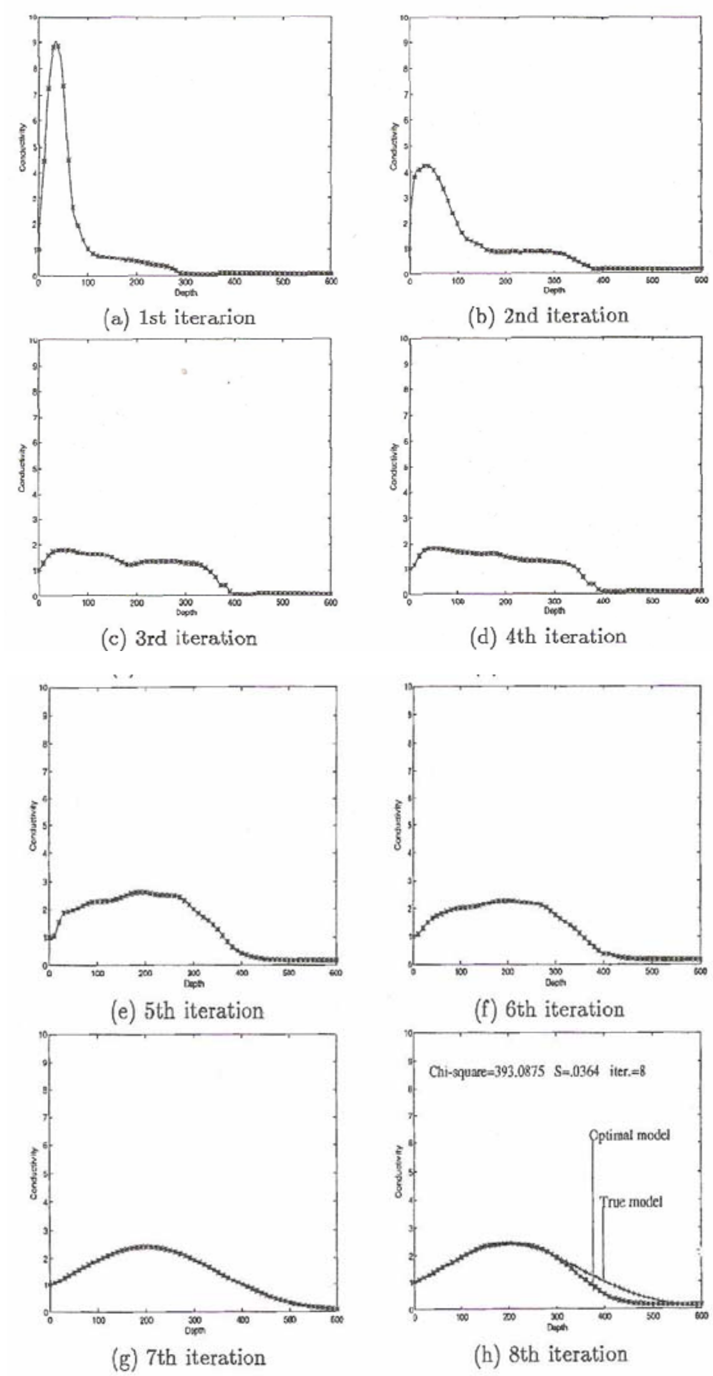

Figure 7.3. Improvement of iteration process from the model.

show the acceptable models starting with two different conductivity profiles and they are obtained after 8 iterations. Thus, the speed of convergence does not depend on the starting model. Backus and Gilbert [2] showed that there exists infinitely many conductivity structures, which are linearly close to $\sigma(z)$, whose calculated responses agree with the observations and that these models differ from each other in their fine scale features. In our examples, we will apply the edgehog method to assess the resolution and the uncertainty in the optimal solutions. In our models, Equation (6.11) is used to determine the parameter q that satisfies a threshold value of $t_q = 0.1$.

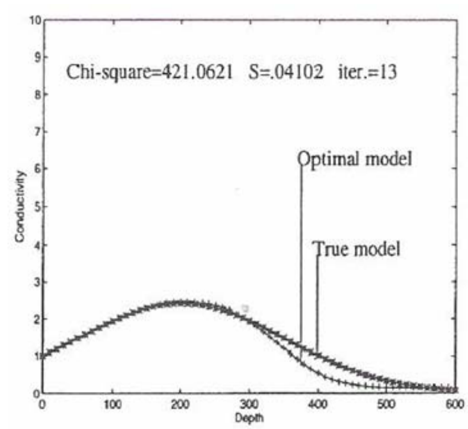

Figure 7.4. Curve of acceptable solution for our model using tangential electric field.

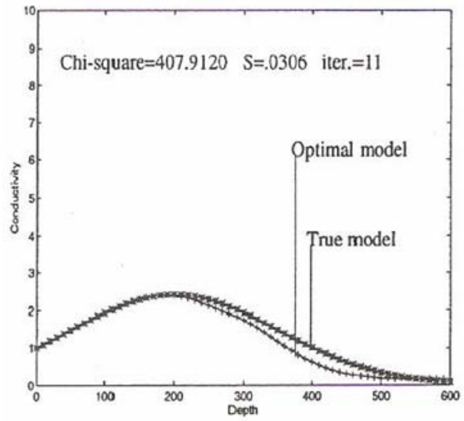

Figure 7.5. Curve of acceptable solution for our model using vertical magnetic field.

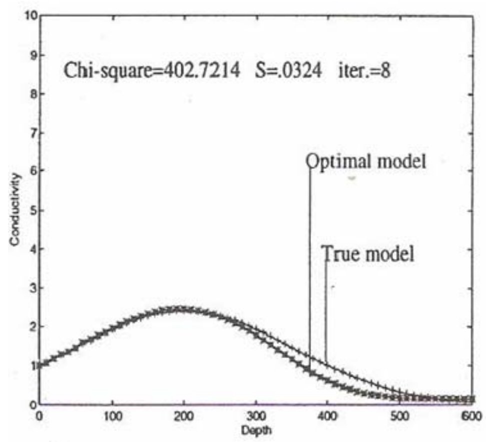

Figure 7.6. Curve of acceptable solution for our model using joint inversion.

Table 7.1 shows the number of columns required for $\mathrm{Var}(x_i^*)$ to remain below the threshold value for each i for our model. Here, we need $q = 13$. Therefore, thirteen principal axes are used for considering the resolution and uncertainty. More axes may be used, if the limit on the variances in x_i^* are allowed to be greater than 0.1.

Table 7.1. Numbers of column used (q) in matrix **V** and variance in x^* limited by threshold value $t_q = 0.1$ for model 1

x_i^*	No. of q	Variance	x_i^*	No. of q	Variance	x_i^*	No. of q	Variance
1	30	.0199	35	23	.0862	69	18	.0309
2	27	.0070	36	19	.0965	70	37	.0503
3	26	.0047	37	17	.0405	71	36	.0787
4	27	.0123	38	15	.0472	72	34	.0801
5	45	.0774	39	20	.0889	73	36	.0912
6	26	.0010	40	18	.0961	74	32	.0888
7	42	.0629	41	18	.0735	75	37	.0860
8	24	.0799	42	16	.0885	76	37	.0759
9	33	.0706	43	18	.0548	77	38	.0857
10	15	.0984	44	19	.0978	78	36	.0968
11	19	.0508	45	16	.0674	79	38	.0835
12	15	.0169	46	16	.0813	80	37	.0534
13	14	.0742	47	20	.0796	81	36	.0637
14	14	.0899	48	19	.0901	82	40	.0745
15	18	.0952	49	22	.0746	83	37	.0707
16	17	.0360	50	20	.0801	84	38	.0311
17	15	.0959	51	18	.0755	85	37	.0373
18	15	.0717	52	14	.0749	86	40	.0710
19	19	.0946	53	16	.0910	87	40	.0736
20	17	.0711	54	17	.0495	88	37	.0529
21	16	.0796	55	21	.0992	89	40	.0978
22	16	.0425	56	15	.0572	90	40	.0917
23	18	.0347	57	18	.0834	91	39	.0329
24	17	.0841	58	13	.0201	92	40	.0966
25	16	.0499	59	19	.0367	93	39	.0825
26	18	.0951	60	20	.0947	94	38	.0142
27	21	.0980	61	21	.0345	95	38	.0337
28	18	.0999	62	36	.0896	96	41	.0595
29	17	.0564	63	31	.0937	97	39	.0912
30	20	.0989	64	21	.0534	98	40	.0738
31	17	.0808	65	22	.0908	99	49	.0665
32	19	.0828	66	20	.0945	100	42	.0508
33	18	.0973	67	33	.0967	101	49	.0884
34	19	.0968	68	20	.0398			

Figure 7.7(a) shows the optimal profile lying between the edge models corresponding to a perturbation of the principal axis. Very little difference is observed when the second to the eighth principal axes were perturbed. The variations start to become significant when the ninth principal axes is perturbed. Figure 7.7(b) to Figure 7.7(d) gives the bounds in the edge models corresponding to perturbing the 9th, 11th, and 13th principal axes. The optimal solution lies about halfway between the two curves in each case. An envelope of the conductivity profile obtained by choosing the maximum and minimum values at each depth for the thirteen principal axes is shown in Figure 7.8. Acceptable models may be expected to lie within the confines of the envelope. Figure 7.8 shows that the envelope is very narrow at the shallow depth, $z = 0$ to $z = 100$ meters. This can be interpreted as saying that our solution is a good representation of the true solution in that interval. In other words, the uncertainty is small. We note from Figure 7.8 that, except for the first 100 meters or so, the fluctuations in the perturbed values increase with changes in the conductivity gradient.

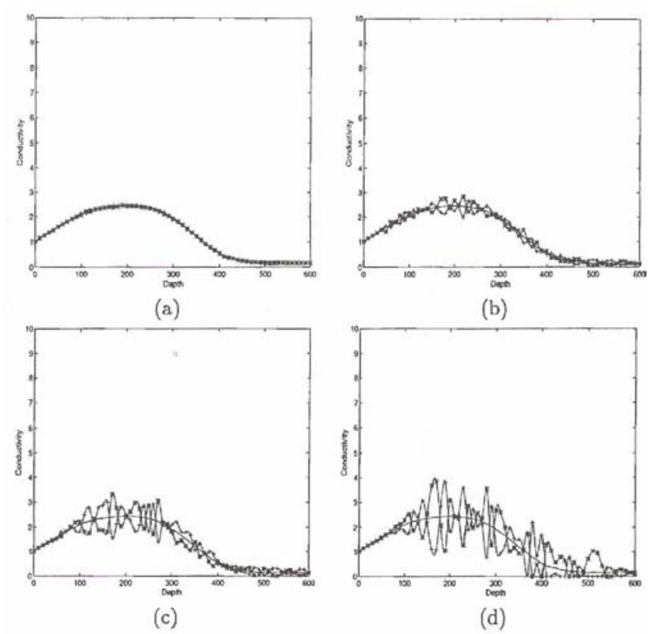

Figure 7.7. Edge model in physical coordinate system transformed from (a) 1st, (b) 9th, (c) 11th, and (d) 13th principal axes.

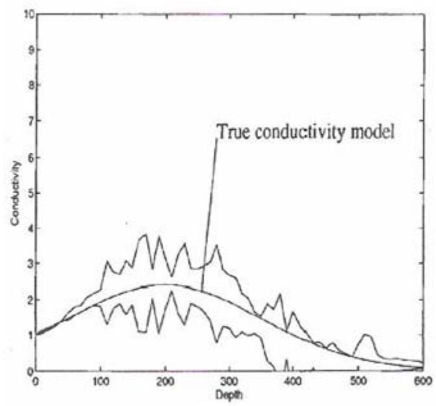

Figure 7.8. Envelope of conductivity profiles for our model in Figure 7.3(h).

8. Conclusion

The inversion of geophysical data is mainly composed of two parts. First, an optimal model must be constructed, which reproduces the observations. Second, the optimal solution so obtained must be appraised to determine how good the resolution is within the range considered. The linearized inverse theory of Backus and Gilbert has been used to construct the matrix, which is used to iteratively obtain the conductivity profile from the starting model. The iterative scheme employs a smoothing filter, which aims to reduce high frequency oscillations and to keep the conductivity structure realistic. Joint inversion has been used and shown to give a faster speed of convergence. In our example, the number of iterations required does not depend on the choice of a starting model. To investigate the resolution in the solution, the edgehog method has been employed to construct the envelope within which possible solutions can lie. The cross section of the envelope describes how good the solution is as a representation of the true model.

Acknowledgement

This research is supported by the Centre of Excellence in Mathematics, the Commission on Higher Education, Thailand, and the Faculty of Science, Silpakorn University, Thailand. The author would like to thank Head of Mathematics Department for the facilities support in our research project as well as Prof. P. F. Siew and Prof. U. C. Das at Curtin University of Technology, Australia for their excellence guidance and comment.

References

[1] G. Backus and F. Gilbert, Numerical applications of a formalism for geophysical inverse problems, Geophysical Journal of the Royal Astronomical Society 13 (1967), 247-276.

[2] G. Backus and F. Gilbert, The resolving power of gross earth data, Geophysical Journal of the Royal Astronomical Society 16 (1968), 199-205.

[3] J. W. Daniel and B. Nobel, Applied Linear Algebra, 3rd ed., Englewood Cliffs, Prentice Hall, NJ, 1988.

[4] U. C. Das, Apparent conductivity curves in controlled-source electromagnetic sounding directly reflecting true resistivities in a layered earth, Geophysics 60 (1995), 53-60.

[5] P. K. Fullagar and D. W. Oldenburg, Inversion of horizontal loop electromagnetic frequency soundings, Geophysics 60 (1984), 150-164.

[6] D. D. Jackson, Marginal solutions to quasi-linear inverse problems in geophysics: The edgehog method, Geophysical Journal of the Royal Astronomical Society 35 (1973), 121-136.

[7] D. L. B. Jupp and K. Vozoff, Stable iterative methods for the inversion of geophysical data, Geophysical Journal of the Royal Astronomical Society 42 (1975), 957-976.

[8] M. A. Meju, Joint inversion of TEM and distorted MT soundings: Some effective practical considerations, Geophysics 61 (1996), 56-65.

[9] D. W. Oldenburg, The interpretation of direct current resistivity measurements, Geophysics 43 (1978), 610-625.

[10] A. P. Raiche, D. L. B. Jupp, H. Rutter and K. Vozoff, The joint use of coincident loop transient electromagnetic and Schlumberger sounding to resolve layered structures, Geophysics 50 (1985), 1618-1627.

[11] R. S. Smith, R. N. Edwards and G. Buselli, An automatic technique for presentation of coincident loop, impulse-response, transient, electromagnetic data, Geophysics 59 (1994), 1542-1550.

[12] K. Vozoff and D. L. B. Jupp, Joint inversion of geophysical data, Geophysical Journal of the Royal Astronomical Society 42 (1975), 977-991.

[13] R. A. Wiggin, The general linear inverse problem, Implication of surface waves and free oscillations for earth structure, Reviews of Geophysics and Space Physics 10 (1972), 251-285.

[14] S. Yooyuanyong and P. F. Siew, The electromagnetic response of a disk beneath an exponentially varying conductive overburden, J. Australian Mathematical Society, Series B 41 (2000), E1-E28.

■